JTTEE5 19:2–10
DOI: 10.1007/s11666-009-9445-8
1059-9630/$19.00 © ASM International

Comparison of In-Flight Particle Properties, Splat Formation, and Coating Microstructure for Regular and Nano-YSZ Powders

A. Elsebaei, J. Heberlein, M. Elshaer, and A. Farouk

(Submitted April 28, 2009; in revised form August 6, 2009)

The relationship between atmospheric pressure plasma spray parameters and in-flight particle characteristics was determined. The morphologies of individual splats and the coating microstructure were studied for different stand-off distances and arc currents. Coating cross-sectional analysis showed that the total porosity of the coating increased with decreasing arc current, and increasing stand-off distance. Two different materials were used: the regular (r-YSZ) feed stock and the nano size (n-YSZ) agglomerated powder. The results illustrate that the r-YSZ coating has higher total porosity at higher arc currents than n-YSZ coating. The splat flattening degree and circularity was examined at different substrate temperatures for both powders. The results indicate that the flattening degree increased at high temperatures for the two materials, but the values for n-YSZ were higher than those for the r-YSZ. This study showed the operating regimes in which the use of n-YSZ yields improved coating properties.

Keywords APS coatings, influence of spray parameters, nano-powders, porosity of coatings, splat formation

1. Introduction

Atmospheric plasma spraying with yttria-stabilized zirconia (YSZ) powders is being widely used for thermal barrier coatings (TBCs) for gas turbines and internal combustion engines (Ref 1). Yttria-stabilized zirconia coatings exhibit low thermal diffusivity, strong adherence to the substrate, phase stability, and thermal shock resistance during thermal cycling, providing oxidation protection to both the metallic bond coat and the substrate. Many studies have contributed to a better understanding of the microstructure, thermal conductivity and diffusivity, residual stresses, and failure mechanisms of the YSZ coatings (Ref 2, 3). The influences of the plasma spray process parameters on the coating characteristics and properties have generally been studied by means of classical one-factor-at-a-time analyses. Porosity and microhardness are two of the basic and key factors to characterize the microstructure and properties of thermal spray coatings. Recently, some online particle monitoring systems (DPV2000) have been developed to measure the temperature and velocity of in-flight particles and to correlate them with the coating quality (Ref 4, 5). In thermal spray, the deposit is built up by successive impacts of molten droplets. The splat microstructure and the contact between the splats and the substrate surface depend on some parameters such as the particle properties in flight, the degree of melting, and the chemical state. The morphology of the splats depends on many parameters, including particle velocity, particle temperature, substrate surface roughness, and substrate temperature (Ref 6). In this study, two types of ceramic powders have been used: one is the regular feed stock 7%YSZ (AI1075, Praxair Inc.) and the other type is nano-YSZ (Nanox S4007, Inframat Inc.). The nano-YSZ powder consists of agglomerations of particles in the 50-100 nm range. The size distribution for the nano-agglomerates was given by the manufacturer as 15-150 μm, but our measurements showed that the majority of the particles were in the range 20-40 μm. Figure 1 shows a micrograph comparing the regular YSZ with the nano-YSZ. We have shown previously that the nano-YSZ can keep a nano-phase morphology during the spray process when the majority of the particles are deposited in a semi-molten state (Ref 7). The cross section of the coatings obtained with the two powders has been analyzed to quantify the crack density, pore porosity, and total porosity for different experimental conditions. The splat morphology for each powder has been studied to calculate circularity and flattening degree.

This article is an invited paper selected from presentations at the 2009 International Thermal Spray Conference and has been expanded from the original presentation. It is simultaneously published in *Expanding Thermal Spray Performance to New Markets and Applications: Proceedings of the 2009 International Thermal Spray Conference*, Las Vegas, Nevada, USA, May 4-7, 2009, Basil R. Marple, Margaret M. Hyland, Yuk-Chiu Lau, Chang-Jiu Li, Rogerio S. Lima, and Ghislain Montavon, Ed., ASM International, Materials Park, OH, 2009.

A. Elsebaei, Mechanical Engineering Department, University of Minnesota, Minneapolis, MN and Faculty of Engineering, Zagazig University, Zagazig, Egypt; **J. Heberlein**, Mechanical Engineering Department, University of Minnesota, Minneapolis, MN; and **M. Elshaer** and **A. Farouk**, Faculty of Engineering, Zagazig University, Zagazig, Egypt. Contact e-mail: jvrh@me.umn.edu.

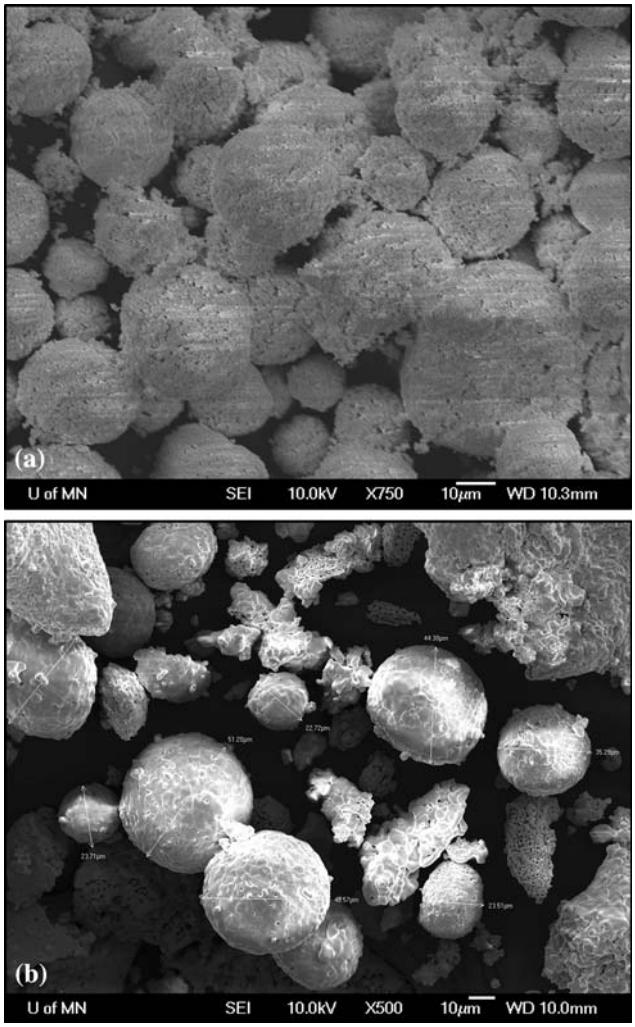

Fig. 1 Comparison of micrographs of the regular YSZ and the nano-YSZ powders

In addition to the coating and splats, the particle in-flight velocity and temperature have been measured, and correlations have been obtained for all data.

2. Experimental Procedure

The SG-100 (Praxair TAFA, Concord, NH) was used as a plasma torch, and carbon steel substrates were used. For splat collection, the substrate was mirror polished in the lab, and then cleaned in an ultrasonic cleaner; the surface roughness was Ra ~ 0.1 μm. The particle temperatures and velocities were measured with the DPV2000. The shutter system used for the splat collection consists of two rotating disks: one holding the substrate, the other containing small holes distributed on the circumference of the disk to let pass single particles for being collected on the substrate. The shutter disk rotates and is moved horizontally when powder injection is started to cover the substrate (see Fig. 2). A fast pyrometer (Marathon MM, Raytek, CA) was used to measure the substrate temperature during the splat collection process. The spraying parameters are summarized in Table 1.

3. In-Flight Particle Diagnostics

The distribution of the particle velocities of r-YSZ and n-YSZ is shown in Fig. 3(a) as a function of the number of particles relative to the total number of particles. The maximum particle velocity is found at the centerline because of the highest momentum transfer at the center (Ref 8). As the vertical position relative to the flame centerline changes downward with particle injection from the top, the particle velocity decreases because larger particles are found on the side opposite from the injection port. The temperature distribution of n-YSZ at the center of the plasma plume indicates that this powder has higher values at the same position compared to the r-YSZ, as shown in Fig. 3(b). This is due to a large number of smaller particles in the n-YSZ powder reaching higher temperatures.

Figure 4 shows the temperature and velocity distributions of the particles at currents of 700 and 870 A. It can be seen that the velocity distributions broadens at higher currents with significantly more number of particles at higher velocities. The temperature distributions are very similar at the different currents, but at the higher current the distribution is shifted toward higher values.

Table 2 shows the average values of particle velocity and temperatures for the n-YSZ and the r-YSZ powder at different radial positions at an axial distance of 80 mm and a current of 870 A. The particles are injected from the positive *Y* direction. It is clear that the n-YSZ particles are approximately 30 m/s faster than the r-YSZ particles at every location. Similarly, the temperature difference between these two types of particles is similar at all radial positions except being somewhat less at larger positive *Y* values. Also given in Table 2 are the average particle diameters as obtained from the DPV 2000 measurements, and it is apparent that the smaller diameter of the n-YSZ powder provides an explanation for the higher velocity and temperature values. As expected, the measured diameter values increase from the positive *Y* direction toward the negative *Y* direction.

4. Coating Characteristics

4.1 r-YSZ Cross Section Coating Microstructure

In order to study the microstructure of cross sections of the coatings, the samples were encapsulated in epoxy to penetrate the pores and cracks. The samples were then cut and polished. The polishing of the cross sections was done using SiC papers with successively finer grits of 320, 500, and 1200, each for 45 s at 300 rpm with recycled water. In the next step, SiC papers of 2400 and 4000 grit were used successively, each for 30 s at 300 rpm with recycled water to remove scratches from the previous polishing steps. After this step, the samples were rinsed with water to

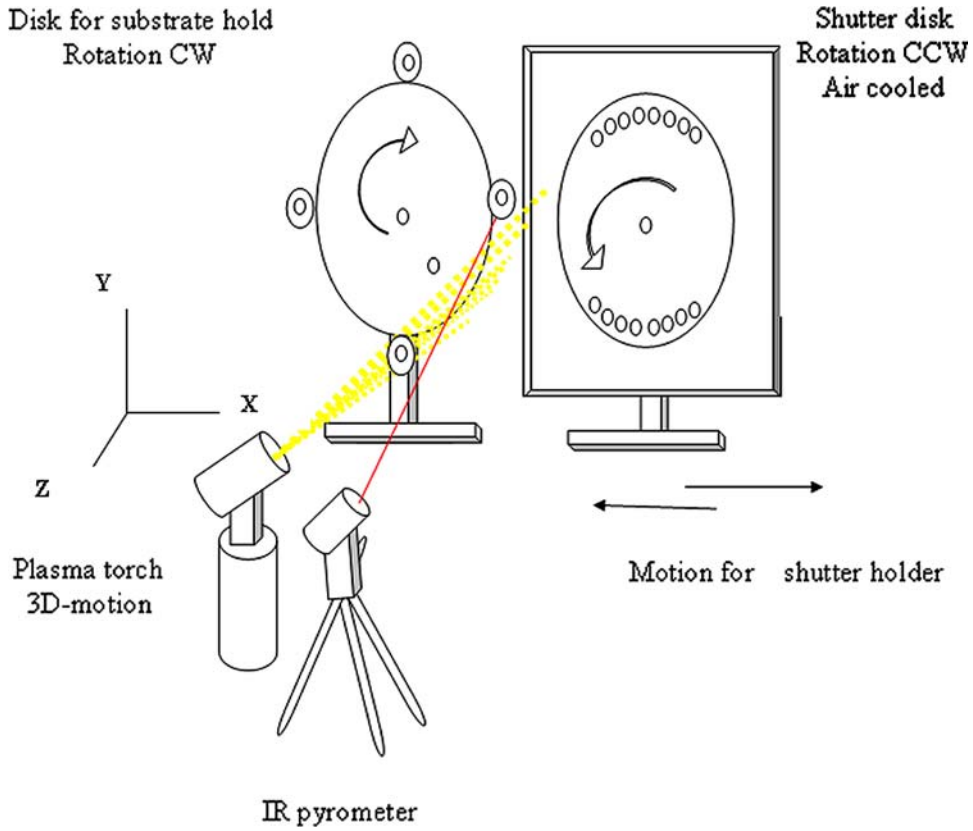

Fig. 2 Experimental setup to coating and splat collection

Table 1 Experimental conditions for the SG-100 DC plasma torch

Arc current, A	870, 700
Primary plasma gas Ar, SLM	55.9
Secondary plasma gas He, SLM	7.1
Carrier gas flow rate Ar, SLM	3.4
Powder feed rate, g/min	7.4
Stand-off distance, mm	80, 100

remove the SiC grit and then dried with air. In the next step, a diamond polishing was performed, first using a 3-micron disk for 2 min at 150 rpm, followed by a polishing with a 1-micron disk for 2 min at 150 rpm, using alcohol for cleaning. The final step consisted of using an OPS (mechanic-chemical) solution for 45 s at 150 rpm. For all polishing, equipment from STRUERS Inc, USA was used. After the polishing process, the samples were coated with platinum with a thickness of about 50 Å to prevent charging in the electron microscope.

Figure 5(a) and (b) show that as the arc current decreases from 870 to 700 A, the number of pores and pullouts increases due to the decrease in the particle temperatures and substrate temperature. The density of cracks increases in the case of lower arc currents due to the increase in the number of fingers of the splats forming these coatings. The other parameter that was observed to affect the coating was the stand-off distance between the torch exit and the substrate. Figure 5(c) and (d) show that as the stand-off distance is decreased from 100 to 80 mm, the number of pores decreases due to the increase in the particle temperature and velocity, leading to a higher flattening degree of the splats due to the decrease in the dynamic viscosity of the material. The pullout density increased at higher stand-off distance as shown in case (d) due to the solidification of some particles.

4.2 n-YSZ Cross Section Coating Microstructure

Figure 6(a) and (b) indicate that the pore density decreases with the increase in the arc current, and the pore density is lower if it is compared to the r-YSZ coating at the same condition probably principally due to the smaller average size of the particles. The crack density decreases with the increase of arc current due to the increase in the particle temperature and substrate temperature. Figure 6(c) and (d) show that the density of pullouts increased at higher stand-off distances as the particle temperature decreases, while the increase in crack density can be related to a decrease in particle velocity.

5. Porosity Analysis

For the determination of the porosity, about 15 images were analyzed from different parts of the coating cross section for both the r-YSZ and the n-YSZ. A Matlab code

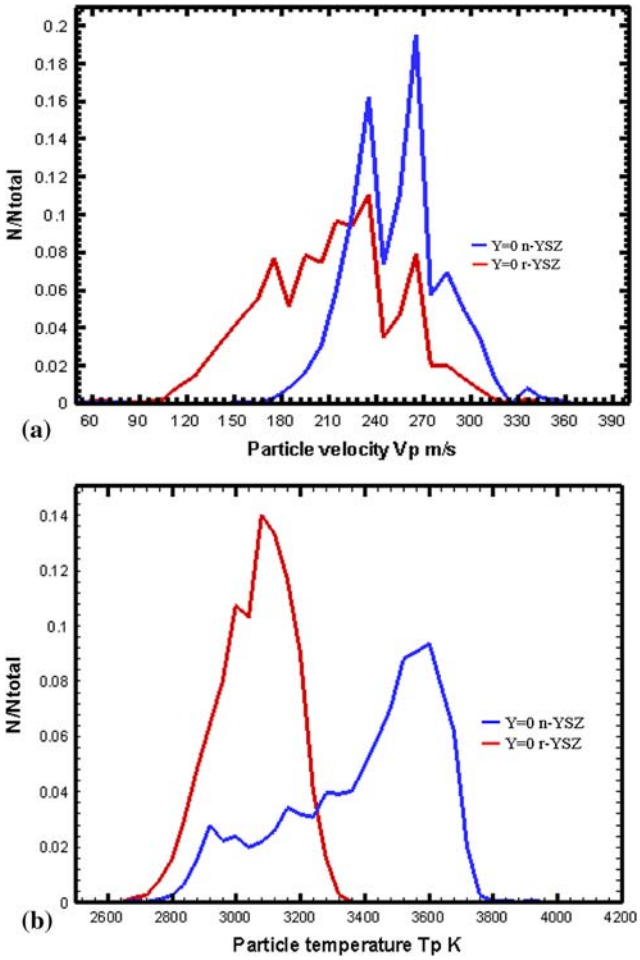

Fig. 3 (a) Particle velocity distribution and (b) temperature distribution for r-YSZ and n-YSZ at the plasma plume centerline $Y = 0$, stand-off distance $D = 80$ mm, $I = 870$ A

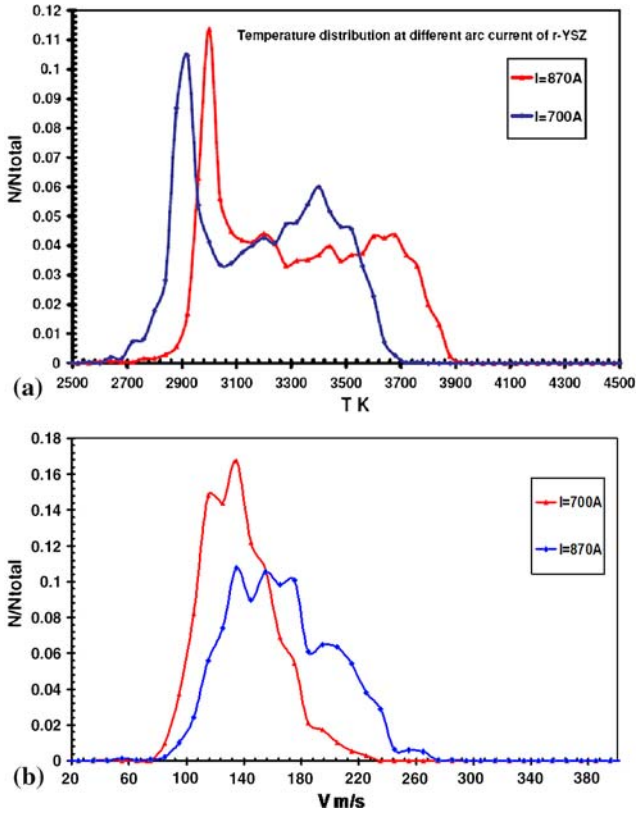

Fig. 4 (a) Particle velocity and (b) particle temperature distributions of r-YSZ at the jet center line ($Y = 0$) at an axial distance $D = 80$ mm for the two arc currents, $I = 700$ A and $I = 870$ A

was then used for the analysis of each of the images, yielding the crack density, pore density (including pull-outs), and total porosity. All images had approximately the same magnification. The results are presented in Table 3. In this table, the first row of data indicates the average number of cracks or pores per image, the second row of numbers shows the average porosity values, and in the third row, the standard deviations for the porosity data are presented. When the standard deviation values are relatively large, the differences between the r-YSZ and the n-YSZ are clearly visible, and the trends of decreasing porosity with increasing current and decreasing stand-off distance are also clear.

6. Splat Morphology

6.1 r-YSZ Splat Morphology

Figure 7(a) and (b) show the splats of r-YSZ at different arc currents but at the same stand-off distance of 80 mm, indicating that with an increase of the arc current the splat morphology changes from a fragmented shape at $I = 700$ A to a uniform disk shape at $I = 870$ A. The reason for the change from a fragmented to a disk shape is the increase of the substrate temperature combined with the increase in particle temperature. The number of fingers can be noticed to decrease with the higher arc current due to the increase in the substrate temperature (Ref 9). Figure 7(c) and (d) indicate that with decreasing stand-off distance from $D = 100$ to $D = 80$ mm the number of fingers decreased due to the increase in the particle impact velocity, combined with the higher substrate temperature. In both cases, the same arc current $I = 870$ A was used.

6.2 n-YSZ Splat Morphology

Figure 8(a) and (b) show that the shape of the n-YSZ is more likely to be disk-shaped with less fingers at higher arc currents compared to the case at lower current. These cases at different arc currents exhibit a lower number of fingers compared to the same cases for r-YSZ. This is likely due to the smaller grain size and the thermophysical properties of n-YSZ (Ref 10). The number of fingers could be lower for n-YSZ at higher stand-off distance $D = 100$ mm as shown in Fig. 8(c) and (d) compared to the same cases for r-YSZ. This is due to the smaller size of the n-YSZ particles with higher particle temperatures making the splats spread more uniformly with less fingers. It is likely that the higher circularity and flattening degree of the n-YSZ splats result in lower coating porosity.

Table 2 Average values of the particle velocity and temperature of the r-YSZ and n-YSZ at different radial positions from the plasma jet center line at an arc current of 870 A and 80-mm stand-off distance

Radial position *Y*, mm	Average particle velocity of r-YSZ, m/s	Average particle velocity of n-YSZ, m/s	Average particle temperature of r-YSZ, K	Average particle temperature of n-YSZ, K	Average particle diameter of r-YSZ, μm	Average particle diameter of n-YSZ, μm
50	236	257	3310	3490	25.7	20.8
40	247	274	3342	3543	26.3	21.4
30	254	284	3392	3565	27.8	22.5
20	248	269	3430	3602	30.3	23.4
10	233	261	3420	3630	32.3	25.3
0	228	256	3400	3620	36.5	26.8
−10	215	245	3340	3576	37	27.6
−20	209	240	3310	3539	38.2	28.7
−30	199	231	3294	3513	42.3	29.8
−40	191	227	3270	3499	44.3	31.1
−50	188	220	3250	3485	45.6	32.1

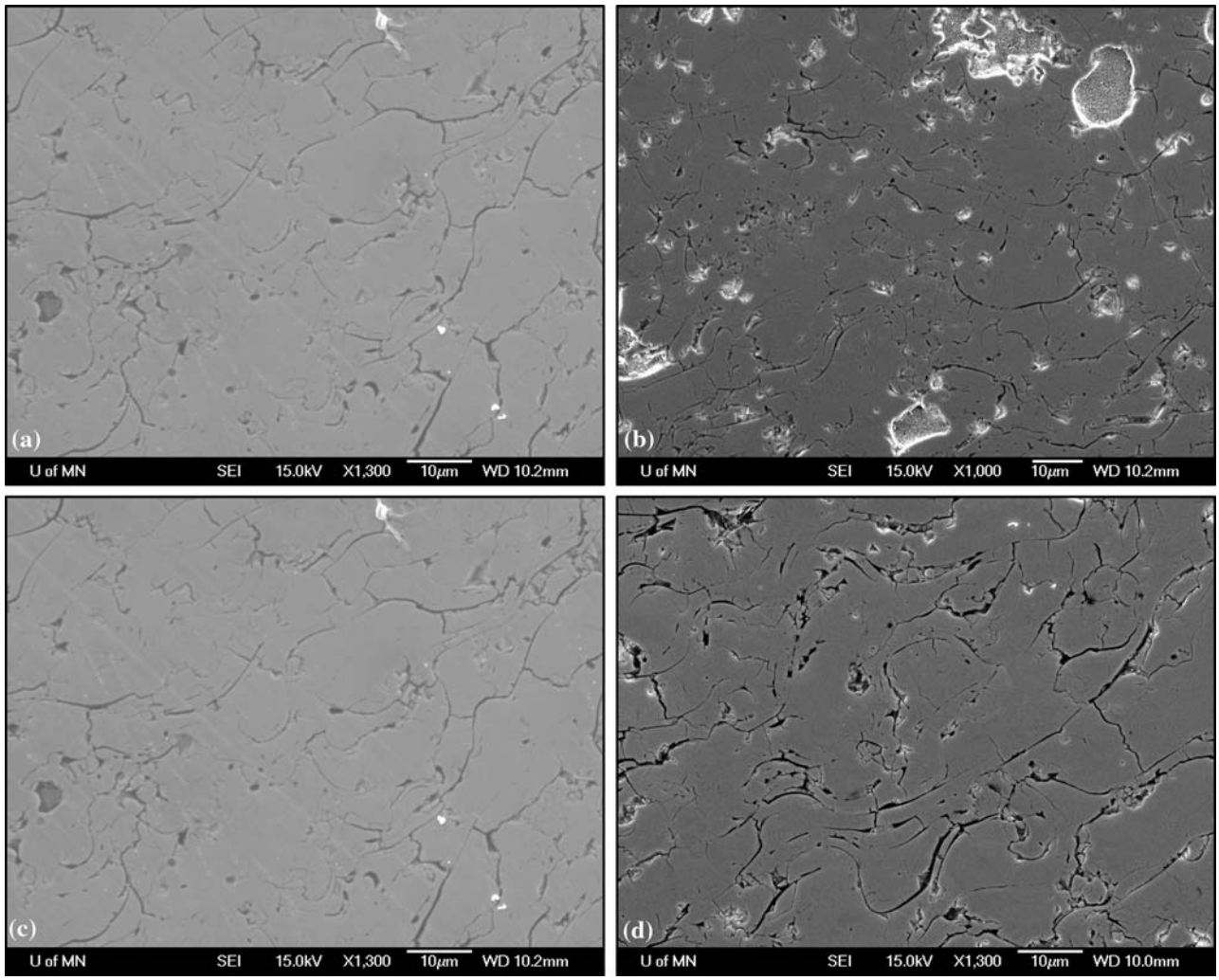

Fig. 5 SEM images of the cross sections with coatings of r-YSZ at: (a) 870 A, (b) 700 A, both at $D = 80$ mm, and (c) $D = 80$ mm, (d) $D = 100$ mm, both at $I = 870$ A

6.3 Splat Analysis

In order to quantify the parameters of the splats collected for r-YSZ at different arc currents and stand-off distances, commercial software (Image J, National Institutes of Health (NIH), MD) was used for image analysis to measure the circularity, while the flattening degree was

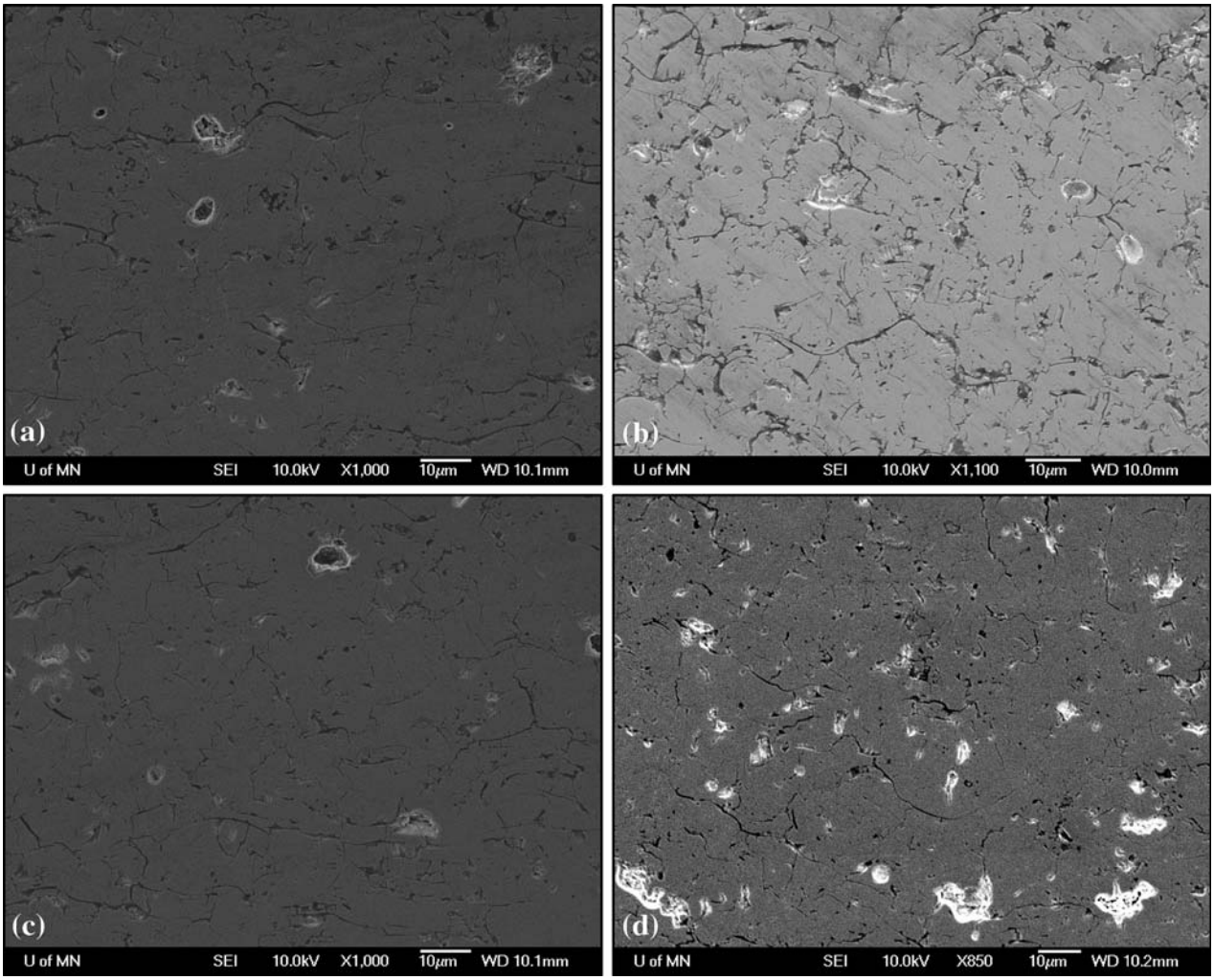

Fig. 6 SEM images cross-section coatings of n-YSZ at (a) 870 A, (b) 700 A, both at $D = 80$ mm, (c) $D = 80$ mm, and (d) $D = 100$ mm, both at $I = 870$ A

Table 3 Porosity analysis for YSZ coating cross-sections

	1. Number of cracks, ave. 2. Crack porosity ave.% 3. Std. dev.		1. Number of pores, ave. 2. Pore porosity ave.% 3. Std. dev.		1. Total porosity ave.% 2. Std. dev.	
Sample code	**r-YSZ**	**n-YSZ**	**r-YSZ**	**n-YSZ**	**r-YSZ**	**n-YSZ**
$I = 870$ A	42	13	95	50		
$D = 80$ mm	0.43	0.19	0.98	0.52	1.41	0.71
	0.21	0.097	0.26	0.23	0.37	0.28
$I = 700$ A	47	31	134	129		
$D = 80$ mm	0.68	0.48	2.44	2.1	3.12	2.5
	0.39	0.189	0.677	0.33	0.57	0.33
$D = 80$ mm	42	13	95	50		
$I = 870$ A	0.43	0.19	0.98	0.52	1.41	0.71
	0.21	0.097	0.26	0.23	0.37	0.28
$D = 100$ mm	72	34	129	96		
$I = 870$ A	0.53	0.37	2.1	1.4	2.63	1.77
	0.22	0.19	0.92	0.47	1.05	0.66

calculated after the measurements of the splat diameters. The data are summarized in Table 4 indicating the differences between splat parameters for r-YSZ and n-YSZ and for different spray parameters. The average values and the standard deviations are also given in this table. It is evident that the n-YSZ splats exhibit an increase in

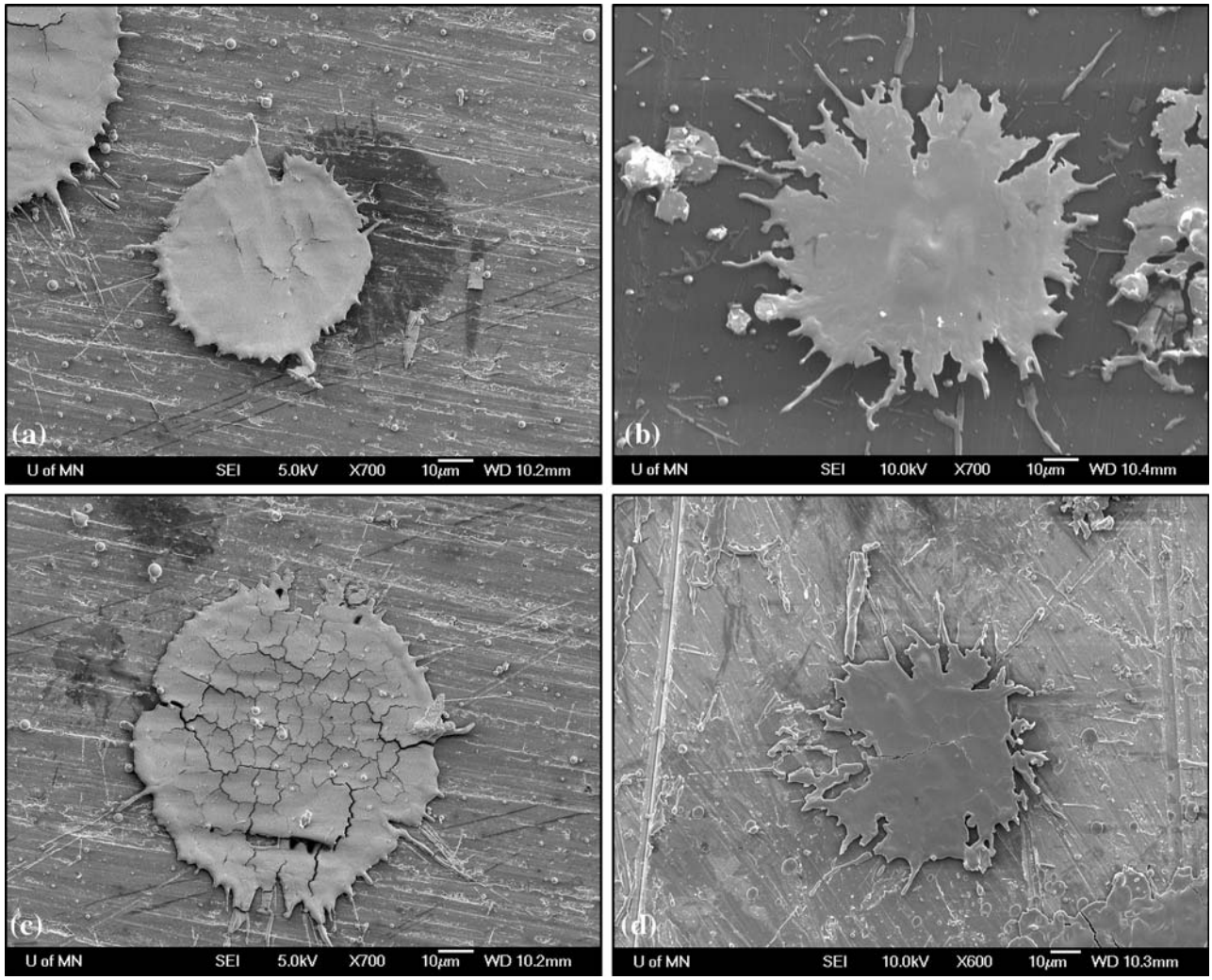

Fig. 7 SEM images for r-YSZ splats at (a) 870 A and (b) 700 A, both at $D = 80$ mm; (c) $D = 80$ mm and (d) $D = 100$ mm, both at $I = 870$ A

circularity and flattening degree compared to the r-YSZ, and that this difference is more pronounced at higher currents (and higher substrate temperatures). This increase in the circularity and flattening degree of n-YSZ splats is likely due to smaller particle size, higher particle temperature, and higher velocity of the n-YSZ particles (Ref 11). The differences in splat diameter are less clear because the wide size distributions lead to large standard deviations.

7. Summary and Conclusion

There is a significant influence of the processing conditions on the properties of plasma-sprayed YSZ coatings. Feed stock particle size, particle condition in the plasma (particle temperature and velocity), and deposition conditions (substrate temperature) have been identified as critical parameters that influence the microstructure and properties. It is observed that the increase in the arc current yields an increase in particle temperature leading to a decrease in the number of pores and cracks inside the coatings. As the stand-off distance increases, the temperature of the particles and velocity decrease, and large pores and more pullouts are seen. The particle size of the n-YSZ is smaller than the size of the r-YSZ, and so the total porosity of n-YSZ coating is lower than that of the r-YSZ coating at the optimum stand-off distance, 80 mm. As the stand-off distance increases, the temperatures of the n-YSZ particles decrease faster, and the total porosity is higher than that of the r-YSZ. Also, the number of unmolten particles is increased. The splats of n-YSZ are more disk shaped at higher stand-off distance due to the higher particle velocity compared to those of r-YSZ. The circularity and flattening degree of n-YSZ splats are larger than those of r-YSZ, at higher arc currents due to higher particle temperatures and higher particle velocities.

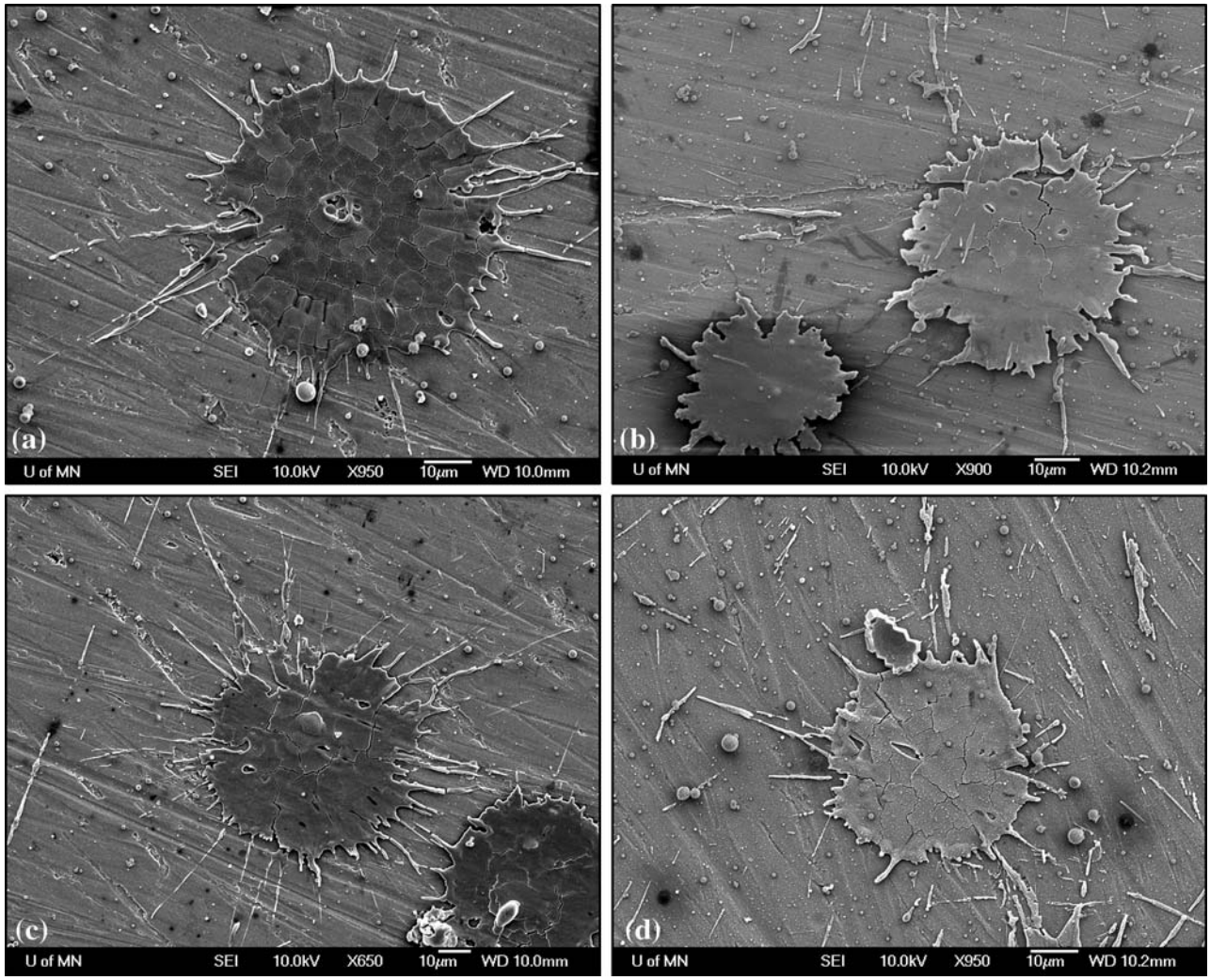

Fig. 8 SEM images for n-YSZ splats at (a) 870 A and (b) 700 A, both at $D = 80$ mm; and (c) $D = 80$ mm and (d) $D = 100$ mm, both at 870 A

Table 4 Summary of results from splat analyses for $D = 80$ mm and $I = 870$, 700 A; and for $I = 870$ A and $D = 80$, 100 mm

	Circularity 1. Ave. value 2. Std. dev.		Splat diameter, μm 1. Ave. value 2. Std. dev.		Flattening degree 1. Ave. value 2. Std. dev.	
Sample code	**r-YSZ**	**n-YSZ**	**r-YSZ**	**n-YSZ**	**r-YSZ**	**n-YSZ**
$I = 870$ A, $D = 80$ mm	0.82	0.93	78.6	85.3	2.45	4.2
Substrate temperature 364 °C	0.05	0.06	12.7	10.2	0.39	0.73
$I = 700$ A, $D = 80$ mm	0.71	0.73	58.6	68.2	1.85	2.63
Substrate temperature 287 °C	0.16	0.12	13.9	11.7	0.4	0.67
$D = 80$ mm, $I = 870$ A	0.82	0.93	78.6	85.3	2.45	4.2
Substrate temperature 364 °C	0.06	0.04	12.7	10.2	0.39	0.73
$D = 100$ m, $I = 870$ A	0.71	0.76	70.4	73.4	1.67	2.82
Substrate temperature 310 °C	0.11	0.09	11.7	10.1	0.24	0.61

Acknowledgments

This research was supported by University of Minnesota, ME department, HTPL laboratories, and Zagazig University, faculty of Engineering, Physics & Math department, in conjunction with the Egyptian Ministry of Higher Education through a joint supervision program.

References

1. A. Anand Kulkarni, A. Vaidya, A. Goland, S. Sampath, and H. Herman, Processing Effects on Porosity-Property Correlations in Plasma Sprayed Yttria-Stabilized Zirconia Coatings, *J. Mater. Sci.*, 2003, **A359**, p 100-111
2. M. Friis, C. Persson, and J. Winer, Investigation of Particle In-Flight Characteristics During Atmospheric Plasma Spraying of Yttria Stabilized ZrO_2: Part 1 Experimental, *J. Surf. Coat. Technol.*, 2001, **141**, p 114-127
3. J.F. Li, H.L. Lioao, C.X. Ding, and C. Coddet, Optimizing the Plasma Spray Process Parameters of Yttria Stabilized Zirconia Coatings Using a Uniform Design of Experiment, *J. Mater. Proces. Technol.*, 2005, **160**, p 34-42
4. C. Moreau, P. Gougeon, M. Lamontagne, V. Lacasse, G. Vaudreuil, and P. Cielo, On-Line Control of the Plasma Spraying Process by Monitoring the Temperature, Velocity, and Trajectory of In-Flight Particles, *Thermal Spray Industrial Applications*, C.C. Berndt and S. Sampath, Ed., *Proc. National Thermal Spray Conference*, June 20-24, 1994 (Boston, MA), ASM International, 1994, p 431-437
5. J. Blain, F. Nadeau, L. Pouliot, C. Moreau, P. Gougeon, and L. Leblanc, An Integrated Infrared Sensor System for On-line Monitoring of Thermally Sprayed Particles, *Surf. Eng.*, 1997, **13**, p 420-424
6. L. Bianchi, A.C. Legger, M. Vardelle, A. Vardelle, and P. Fauchais, Microstructuctural Investigation of Plasma-Sprayed Ceramic Splats, *J. Thin Solid Films*, 1996, **305**, p 35-37
7. D.N. Guru and J.V.R. Heberlein, Plasma Spray Processing of Nanostructures Partially Stabilized Zirconia for a Strain Accommodating Inter-Layer—Splat Characteristics, *Proc. ITSC 2008,* June 2-4, 2008 (DVS Verlag, Düsseldorf, Germany; Maastricht, Netherlands), unpaginated CD
8. Y.J. Su, T.F. Bernecki, and K.T. Faber, In Situ Characterization of Small-Particle Plasma Sprayed Powders, *J. Therm. Spray. Technol.*, 2002, **11**(1), p 52-61
9. S. Sampath, X.Y. Jiang, J. Matejick, A.C. Leger, and A. Vardelle, Role of Thermal Spray Processing Method on the Microstructure, Residual Stress and Properties of Coatings: An Integrated Study for Ni-5wt.%Al Bond Coats, *J. Mater. Sci.*, 1999, **A272**, p 181-188
10. H. Chen, X. Zhou, and C. Ding, Investigation of the Thermomechanical Properties of a Plasma-Sprayed Nanostructured Zirconia Coating, *J. Eur. Ceram. Soc.*, 2003, **23**, p 1449-1455
11. R.S. Lima and B.R. Marple, Thermal Spray Coatings Engineered from Nanostructured Ceramic Agglomerated Powders for Structural, Thermal Barrier and Biomedical Application, *J. Therm. Spray. Technol.*, 2007, **16**(1), p 40-63